Computational Mechanics 33 (2004) 95–107 © Springer-Verlag 2003
DOI 10.1007/s00466-003-0503-7

Generalized finite element method in structural nonlinear analysis – a *p*-adaptive strategy

F. B. Barros, S. P. B. Proença, C. S. de Barcellos

Abstract This paper is concerned with an extension of the generalized finite element method, GFEM, to nonlinear analysis and to the proposition of a *p*-adaptive strategy. The *p*-adaptivity is considered due to the nodal enrichment scheme of the method. Here, such scheme consists of multiplying the partition of unity functions by a set of polynomials. In a first part, the performance of the method in nonlinear analysis of a reinforced concrete beam with progressive damage is presented. The adaptive strategy is then proposed on basis of a control over the approximation error. Aiming to estimate the approximation error, the equilibrated element residual method is adapted to the GFEM and to the nonlinear approach. Then, global and local error measures are defined. A numerical example is presented outlining the effectivity index of the error estimator proposed. Finally, a *p*-adaptive procedure is described and its good performance is illustrated by a numerical example.

Keywords Finite element method, Meshless methods, Adaptivity, Error estimation, Nonlinear structural analysis

1 Introduction

The generalized finite element method, (GFEM), [1] and [2], shares several features with the so-called meshless methods. In fact, the approximation functions used in the GFEM are associated with nodal points and the enrichment of the approximation spaces can be done at the nodes in the same fashion as in the meshless *hp*-Cloud method, [3]. But, on the other hand, the partition of unity, [3, 4], used in the GFEM is provided by Lagrangian finite element shape functions. Therefore this method can be understood also as a non-conventional form of the finite element method. Indeed, both interpretations of the GFEM are valid and give unique insights into the method.

The nodal enrichment feature of the GFEM, allowing to avoid mesh refinement is indeed very attractive for nonlinear analysis. The method opens the possibility to improve accuracy without excessively increasing of the computational effort. Among the advantages, one can mention that a mesh refinement may be unnecessary in problems involving stress concentrations, [5, 6]. Numerical locking can also be efficiently affronted by the nodal enrichment. The same feature could be explored in damage or plasticity localization analysis. Moreover, by using customized enrichment functions the fronts of damage or plasticity could be accurately reproduced.

On the other hand, the method naturally suggests an adaptive scheme to provide automatically the nodal enrichment. Accordingly, as the polynomial functions fit very well with the GFEM enrichment strategy, a *p*-refinement can be considered. Therefore, this paper has two objectives: to extend the GFEM to material nonlinear analysis due to progressive damage and to propose a *p*-adaptive strategy tailored to the nonlinear approach.

Regarding the adaptive procedure, the error measure used to control the refinement scheme is evaluated by the element residual method, [7, 8], which is proposed as a global measure and also as a local indicator associated to each cloud. One problem resulting from the such treatment is that the local error problem can result not well posed. Then, the additional condition necessary to guarantee uniqueness of the error problem can be achieved by following the residual equilibration scheme described in [9] and adapted here to the GFEM. In spite of the error issue be developed along the text by considering the elements of the clouds, at the end the consistency with GFEM is recovered, being the adaptive refinement conducted by using nodal error values. Such nodal values are estimated here by a weight mean procedure of the element indicators.

The paper content is outlined as follows. In Sect. 2 and 3 the GFEM and its use on elasticity boundary vale problems are briefly commented. The nonlinear problem is treated in Sect. 4. A reinforced concrete beam is presented in Sect. 5 as a motivation for *p*-adaptivity. The

Received: 7 March 2003 / Accepted: 25 August 2003
Published online: 20 November 2003

F. B. Barros
Department of Structural Engineering,
School of Engineering of Federal University of Minas Gerais,
Av. Contorno 842, Belo Horizonte, M.G., Brazil

S. P. B. Proença (✉)
Department of Structural Engineering,
São Carlos School of Engineering,
University of São Paulo, Av. Trabalhador São-carlense,
400, São Carlos, S.P., Brazil, CEP:13566-59
e-mail: persival@sc.usp.br

C. S. de Barcellos
Department of Mechanical Engineering,
Pontifícia Universidade Católica,
Belo Horizonte, M.G., Brazil

The authors gratefully acknowledge the Conselho Nacional de Desenvolvimento Cientifico e Tecnológico (CNPq) at Brazil.

error estimator issue is then addressed in Sect. 6. The implicit element residual method and its use in the GFEM is detailed in this section. In particular, local error indicators and global error estimators are proposed, followed by an analysis of the effectivity index. In the Sect. 7 the *p*-adaptive scheme for nodal refinement is described. A numerical example is then shown in Sect. 7.2 to demonstrate the efficiency of the adaptive proposition. The final considerations and conclusions are presented in sect. 8.

2 The generalized finite element method

According to [2], the GFEM was proposed independently by:

- Babuška and coworkers, initially named as special finite element method, [10], and later as the partition of unity finite element method, [11, 12];
- Duarte and Oden, as a meshless formulation in the *hp*-Cloud method, [13, 14], and later as an hybrid approach with the FEM, [15].

It must be noted that a similar philosofy is inserted in the works of Belytshko, [16, 17], named as extended finite element method (XFEM).

In GFEM, [2], a set of partition of unity (PU) functions is employed to enforce interelement continuity, creating conforming approximations which are improved by a nodal enrichment strategy. This process of constructing approximation functions is described on what follows.

Let us consider, e.g., a conventional mesh of linear finite elements, $\{\mathscr{K}_e\}_{e=1}^{NE}$, defined by N nodes, $\{\mathbf{x}_j\}_{j=1}^{N}$, in a domain Ω, see Fig. 1a. The generic patch or cloud $\omega_j \in \Omega$ is obtained by the union of the finite elements sharing the vertex node $\mathbf{x}_j$. The assemblage of the Lagrangian interpolating functions belonging to each element and associated with the node $\mathbf{x}_j$ compose the function $\mathscr{N}_j$ defined over the support cloud ω_j, Fig. 1b. As $\sum_{j=1}^{N} \mathscr{N}_j = 1$ at each position $\mathbf{x}$ in the domain Ω, the set of functions $\{\mathscr{N}_j\}_{j=1}^{N}$ constitutes a partition of unity. Let us assign the following set of q linearly independent functions, stated to each cloud ω_j as:

$$\mathscr{I}_j \stackrel{\text{def}}{=} \{L_{j1}, L_{j2}, \ldots, L_{jq}\} \stackrel{\text{def}}{=} \{L_{ji}\}_{i=1}^{q} \quad \text{with } L_{j1} = 1 \tag{1}$$

The generalized finite element shape functions associated to the node $\mathbf{x}_j$ result from the enrichment, i.e. the multiplication, of the PU functions of the cloud ω_j by each of the components of (1):

$$\{\phi_{ji}\}_{i=1}^{q} = \mathscr{N}_j \times \{L_{ji}\}_{i=1}^{q} \tag{2}$$

The linear combination leading to such shape functions can be understood by considering the representations depicted in Fig. 1 for the case of approximations defined in $\mathbb{R}^2$. The enrichment scheme is obtained by multiplying a PU function (bi-linear) of C^0-type, Fig. 1b, and presenting compact support ω_j, by the function L_{ji}, Fig. 1c, named in [1] as a local approximation. The resulting shape function ϕ_{ji}, Fig. 1d, inherits characteristics of both functions, e.g., the compact support of the PU and the approximate character of the local function.

For instance, the generalized global approximation for the displacements over Ω, denoted as $\tilde{\mathbf{u}}(\mathbf{x})$, can then be described as a linear combination of the shape functions associated to each node:

$$\tilde{\mathbf{u}}(\mathbf{x}) = \sum_{j=1}^{N} \mathscr{N}_j(\mathbf{x}) \left\{ \mathbf{u}_j + \sum_{i=2}^{q_j} L_{ji}(\mathbf{x}) \mathbf{b}_{ji} \right\} \Rightarrow \tilde{\mathbf{u}} = \mathbf{\Phi}^T \mathbf{U} \tag{3}$$

where $\mathbf{u}_j$ and $\mathbf{b}_{ji}$ are nodal parameters respectively associated with the components $\mathscr{N}_j$ and L_{ji} of the shape functions. The continuity of this function over the entire

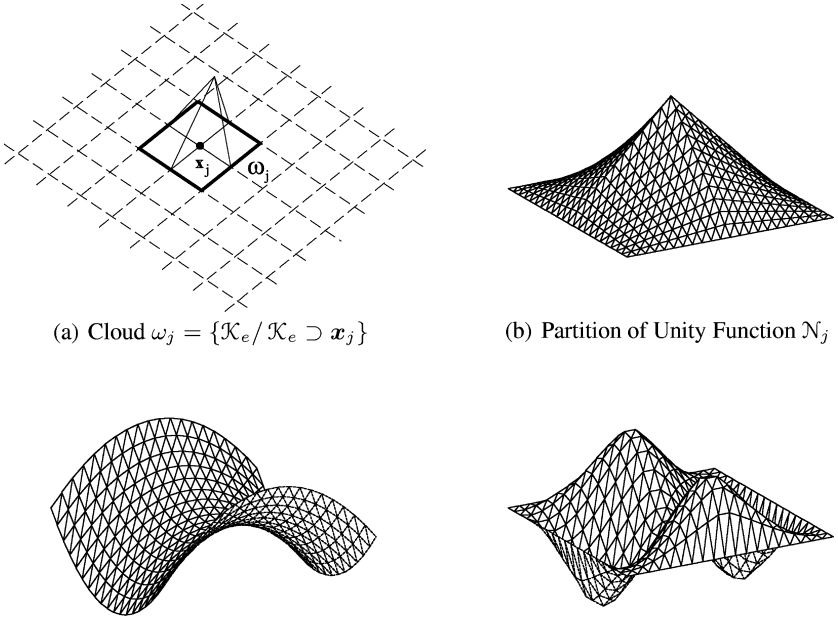

(a) Cloud $\omega_j = \{\mathcal{K}_e / \mathcal{K}_e \supset \boldsymbol{x}_j\}$

(b) Partition of Unity Function $\mathcal{N}_j$

(c) Local Approximation Function L_{ji}

(d) Enriched Shape Function $\phi_{ji} = \mathcal{N}_j \times L_{ji}$

Fig. 1. Enrichment scheme of the cloud ω_j

domain is granted by the compact support of the PU ($(\mathscr{N})_j(\mathbf{x}) = 0$ on the boundary of ω_j). The special functions L_{ij} determine the local character of the resulting approximation.

3
The Boundary value problem–fundamental equations

Let us consider the linear elasticity boundary value problem, BVP, defined in the domain $\Omega \in \mathbb{R}^2$ where a reference system x-y is attached.

$$\text{Find } \mathbf{u} \text{ such that: } \begin{cases} \nabla^T \boldsymbol{\sigma}(\mathbf{u}) + \mathbf{b} = \mathbf{0} & \text{in} \quad \Omega \\ \mathbf{u} = \hat{\mathbf{u}} & \text{on} \quad \Gamma_D \\ \mathbf{t}(\mathbf{u}) = \hat{\mathbf{t}} & \text{on} \quad \Gamma_N \end{cases} \tag{4}$$

where $\mathbf{u}^T \overset{\text{def}}{=} \{u_x \; u_y\}$ is the displacement vector, Γ_D and Γ_N denote complementary parts of the boundary $\partial\Omega$ of the region occupied by the solid in Ω, where the Dirichlet and Neumman conditions are defined respectively, $\boldsymbol{\sigma} = \mathbf{D}\boldsymbol{\varepsilon}$ is the stress tensor, $\boldsymbol{\varepsilon}$ is the strain tensor, $\mathbf{D}$ is the constitutive stiffness tensor, $\mathbf{b}$ is the vector of body forces, $\mathbf{t} = \boldsymbol{\sigma}\mathbf{n}$, is the traction vector, $\hat{\mathbf{u}}$ and $\hat{\mathbf{t}}$ are the prescribed displacement and traction vectors, $\mathbf{n}$ is the unit outward normal to the boundary $\partial\Omega$.

The corresponding variational form of this problem can be stated as:

$$\text{Find } \mathbf{u} \in \mathscr{H}^1(\Omega) \text{ such that:}$$
$$\mathscr{B}(\mathbf{u}, \mathbf{v}) = l(\mathbf{v}) \quad \forall \mathbf{v} \in \mathscr{H}^1(\Omega) \text{ with } \mathbf{u} = \hat{\mathbf{u}} \text{ on } \Gamma_D \tag{5}$$

where $\mathscr{H}^1(\Omega)$, the Hilbert space of degree 1, is the standard Sobolev space of square integrable functions whose first derivatives are square integrable as well, and that is defined on the domain Ω, the following variational operators are defined:

$$\mathscr{B}(\mathbf{u}, \mathbf{v}) = \iint_{\Omega} \boldsymbol{\varepsilon}^T(\mathbf{v}) \boldsymbol{\sigma}(\mathbf{u}) l_z \, dx \, dy$$

$$l(\mathbf{v}) = \iint_{\Omega} \mathbf{v}^T \mathbf{b} l_z \, dx \, dy + \int_{\Gamma_N} \mathbf{v}^T \hat{\mathbf{t}} l_z \, ds$$

$\mathbf{v}^T \overset{\text{def}}{=} \{v_x \; v_y\}$ is the test function vector, $\boldsymbol{\varepsilon}(\mathbf{v})$ is obtained by the gradient operation over $\mathbf{v}$, l_z is the dimension of the elastic body in z reference direction (thickness), considered here as constant.

The Galerkin approximation of (5) corresponds to a solution belonging to the space of finite dimension $\tilde{\mathscr{X}}$ built by the kinematically admissible GFEM shape functions. Thus, the Galerkin approximation results from:

$$\text{Find } \tilde{\mathbf{u}} \in \tilde{\mathscr{X}} \text{ such that: } \mathscr{B}(\tilde{\mathbf{u}}, \tilde{\mathbf{v}}) = l(\tilde{\mathbf{v}}) \quad \forall \tilde{\mathbf{v}} \in \tilde{\mathscr{X}} \tag{6}$$

where $\tilde{\mathbf{u}}$ and $\tilde{\mathbf{v}}$ are obtained from the expression (3) as:

$$\tilde{\mathbf{u}}(\mathbf{x}) = \sum_{j=1}^{N} \mathscr{N}_j(\mathbf{x}) \left\{ \mathbf{u}_j + \sum_{i=2}^{q_j} L_{ji}(\mathbf{x}) \mathbf{b}_{ji} \right\} \Rightarrow \tilde{\mathbf{u}} = \boldsymbol{\Phi}^T \mathbf{U} \tag{7}$$

$$\tilde{\mathbf{v}}(\mathbf{x}) = \sum_{j=1}^{N} \mathscr{N}_j(\mathbf{x}) \left\{ \mathbf{v}_j + \sum_{i=2}^{q_j} L_{ji}(\mathbf{x}) \mathbf{c}_{ji} \right\} \Rightarrow \tilde{\mathbf{v}} = \boldsymbol{\Phi}^T \mathbf{V} \tag{8}$$

The system of equations resulting from (6) is positive semi-definite due to the linear dependency of the set of shape functions. This kind of system can be solved efficiently by the iterative procedure proposed in [2] and [18].

4
Nonlinear analysis

In this work, the nonlinearity is introduced in the BVP by the material constitutive model. The material nonlinear response is related to the propagation of microcracks in concrete and it is modeled on the basis of continuum damage mechanics. The Mazars' damage model presently selected, [19], models the concrete as an elastic medium subjected to progressive damage. On verifying the constitutive model the approach adopted is nonlocal, [20], in order to avoid mesh dependence. Accordingly, a weighted average of the equivalent tensile strains is composed over a region of influence at each reference position and then used in the damage criterion. Such a region is defined by a radius r_{nl} physically associated to the maximum aggregate size.

The resulting nonlinear structural problem can be solved using an incremental and iterative scheme. Thus, by assuming that the solution at the instant t is known, at $t + \Delta t$ the problem to be solved is:

$$\begin{aligned} &\nabla^T \boldsymbol{\sigma}({}^{t+\Delta t}\mathbf{u}) + {}^{t+\Delta t}\mathbf{b} = \mathbf{0} \quad \text{in} \quad \Omega \\ &\mathbf{t}({}^{t+\Delta t}\mathbf{u}) = {}^{t+\Delta t}\hat{\mathbf{t}} \quad \text{in} \quad \Gamma_N \\ &{}^{t+\Delta t}\mathbf{u} = {}^{t+\Delta t}\hat{\mathbf{u}} \quad \text{in} \quad \Gamma_D \end{aligned} \tag{9}$$

The Galerkin approximation of the variational form for the problem (9) can then be searched for. In $\mathbb{R}^2$, denoting by $\mathbf{L}$ the differential operator matrix and by $\mathbf{B}$ the operator which relates displacement vector $\mathbf{U}$ to the strain vector $\boldsymbol{\varepsilon}$:

$$\mathbf{L}^T \overset{\text{def}}{=} \begin{bmatrix} \partial/\partial x & 0 & \partial/\partial y \\ 0 & \partial/\partial y & \partial/\partial x \end{bmatrix} \quad \mathbf{B} = \mathbf{L}\boldsymbol{\Phi}^T \tag{10}$$

the following algorithm is used to obtain the equilibrium iteratively by the Newton-Raphson method:

$$\begin{aligned} &\text{For } i_t = 1, 2, \ldots, \bar{i}_t, \ldots, i_t^{\max} \\ &\boldsymbol{\psi}^{(i_t-1)} = {}^{t+\Delta t}\mathbf{F}_{\text{ext}} - {}^{t+\Delta t}\mathbf{F}_{\text{int}}^{(i_t-1)} \\ &{}^{t+\Delta t}\mathbf{K}_{\text{sec}}^{(i_t-1)} \Delta\mathbf{U}^{(i_t)} = \boldsymbol{\psi}^{(i_t-1)} \\ &{}^{t+\Delta t}\mathbf{U}^{(i_t)} = {}^{t+\Delta t}\mathbf{U}^{(i_t-1)} + \Delta\mathbf{U}^{(i_t)} \end{aligned} \tag{11}$$

where the superscript i_t denotes the iteration and $\Delta U^{(i_t)}$ is the displacement increment. The out-of-balance load vector is represented by $\boldsymbol{\psi}^{(i_t-1)}$, whereas ${}^{t+\Delta t}\mathbf{F}_{\text{ext}}$ is the externally applied nodal force vector and ${}^{t+\Delta t}\mathbf{F}_{\text{int}}$ is the equivalent nodal force to the stress distribution. The following initial conditions must be imposed at the beginning of each time step:

$${}^{t+\Delta t}\mathbf{U}^{(0)} = {}^{t}\mathbf{U}^{(\bar{i}_t)}; \quad {}^{t+\Delta t}\mathbf{K}_{\text{sec}}^{(0)} = {}^{t}\mathbf{K}_{\text{sec}}^{(\bar{i}_t)}; \quad {}^{t+\Delta t}\mathbf{F}_{\text{int}}^{(0)} = {}^{t}\mathbf{F}_{\text{int}}^{(\bar{i}_t)}$$

where $\bar{i}_t$ denotes an iteration in which the convergence criterion is verified.

Considering only plane states and adopting the Mazars' damage model the secant stiffness matrix can be obtained from:

$$^{t+\Delta t}\mathbf{K}_{\text{sec}} = \iint_{\Omega} \mathbf{B}^T(1-D)\mathbf{C}\mathbf{B}l_z \,\mathrm{d}x\,\mathrm{d}y \tag{12}$$

where C is the initial elastic stiffness tensor and $0 < D < 1$ is the scalar variable related to the present deteriorated local state of the material. The nodal force vectors are constructed as follows:

$$^{t+\Delta t}\mathbf{F}_{\text{ext}} = \iint_{\Omega} \mathbf{\Phi}^{t+\Delta t}\mathbf{b}l_z \,\mathrm{d}x\,\mathrm{d}y + \int_{\Gamma_N} \mathbf{\Phi}^{t+\Delta t}\hat{\mathbf{t}}l_z \,\mathrm{d}s \tag{13}$$

$$^{t+\Delta t}\mathbf{F}_{\text{int}}^{i_t} = \iint_{\Omega} \mathbf{\Phi}\boldsymbol{\sigma}(^{t+\Delta t}\mathbf{u}_p)l_z \,\mathrm{d}x\,\mathrm{d}y \tag{14}$$

The convergence criterion for the iterative procedure is based on the energy norm increment given by:

$$\|\Delta\mathbf{u}_p\|_{\mathscr{U}} \overset{\text{def}}{=} \sqrt{\Delta\mathbf{U}^{(i_t)^T}\boldsymbol{\psi}^{(i_t-1)}} = \sqrt{\sum_{i=1}^{\text{NDF}}\left(\Delta U_i^{(i_t)}\psi_i^{(i_t-1)}\right)} \tag{15}$$

where NDF denotes the number of degrees of freedom.

5 Reinforced concrete beam problem as a motivation for *p*-adaptivity

The structural problem to be considered is a simply supported reinforced concrete beam of rectangular cross section depicted in Fig. 2. The loading is composed by two concentrated forces applied symmetrically with respect to the middle section. The region between the applied forces is submitted to an uniform bending then inducing a diffuse damage distribution.

The adopted values for the Mazars's model parameters $(A_T, B_T, A_C, B_C, \varepsilon_{d0})$, the elastic properties for concrete and steel and the radius r_{nl} for the nonlocal approach are as follows:

$A_T = 0.7 \quad B_T = 8000 \quad A_C = 0.85 \quad B_C = 1050$

$\varepsilon_{d0} = 0.00007 \quad E_c = 29200\,\text{MPa} \quad E_s = 196000\,\text{MPa}$

$\nu_c = 0.2 \quad \nu_s = 0.3 \quad r_{\text{nl}} = 3\,\text{cm}$

It must be noted that the Mazars's parameters were identified on the basis of experimental response [21]. A linear elastic behavior is assumed for steel, the concrete and reinforcement are assumed to be perfectly adherent.

Two static simulations where performed on the same structure, one by the conventional FEM and one by GFEM. The finite element meshes defined in each case are shown in Fig. 3, being composed by quadrilateral bilinear elements. Mesh I has 1376 degrees of freedom. On the other hand, in Mesh II a few elements where used aiming to emphasize the GFEM enrichment advantage. The set $\mathscr{I}_j$ of independent functions used in the nodal enrichment is represented as:

$$\mathscr{I}_j = \left\{p_{j1}, p_{j2}, p_{j3}, \ldots, p_{jq_j(p)}\right\} \quad \text{with} \quad p_{j1} = 1 \tag{16}$$

Presently, the parameter $q_j(p)$ corresponds to the number of monomials required to reproduce exactly complete polynomials of p degree, with respect to the global coordinate system. This fact guarantees the polynomial completeness of the approximation, even with meshes of distorted elements (there is no need to be concerned about awkward-looking meshes, as long as the elements present straight sides and, of course, with all interior angles between 0 an 180°). The monomials are bubble like functions presenting null values at node $\mathbf{x}_j$ and are normalized by a characteristic mesh dimension defined as the greatest linear distance among nodes composing the cloud ω_j. The assumptions used in the simulation are as follows:

boundary conditions: prescribed forces and displacement restrictions were imposed in a distributed form over small elements, as indicated in Fig. 3;

reinforcement: in both meshes the steel bars were considered directly in the element formulation [22];

numerical integration: the Gauss-Legendre Quadrature rule was employed. In Mesh I, 2×2 Gauss points were used, whereas 4×4 points were used for Mesh II near at the constraints and at the distributed load. For the rest of elements in Mesh II, 6×6 Gauss points were used in order to properly capture the damage evolution;

non-local analysis: the adopted radius is compatible with concrete analysis and avoids mesh dependence;

tolerance and load steps: in order to control the convergence of the iterative procedure, a tolerance was considered to the incremental energy norm. A constant value of 0.5% related to the first elastic step was adopted aiming to keep the same stop criterion for all the iterative procedure. Due to the strong nonlinearity observed from the loading level of 12 kN, a proper loading path was defined. At the beginning, four load steps were applied, each of them representing 9% of the total loading value

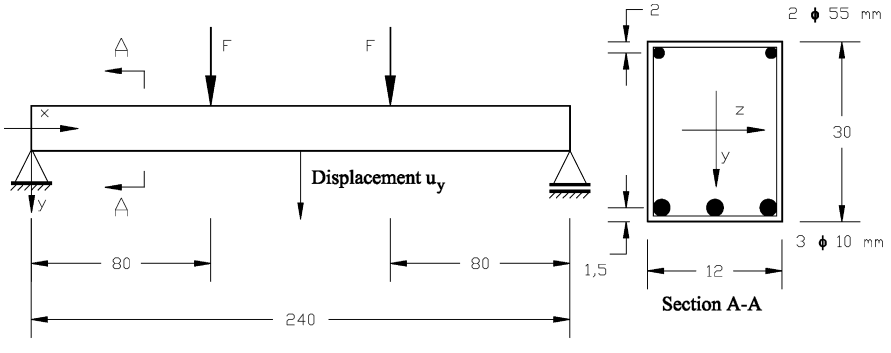

Fig. 2. Reinforced concrete beam–geometry and reinforcement distribution–dimensions in cm

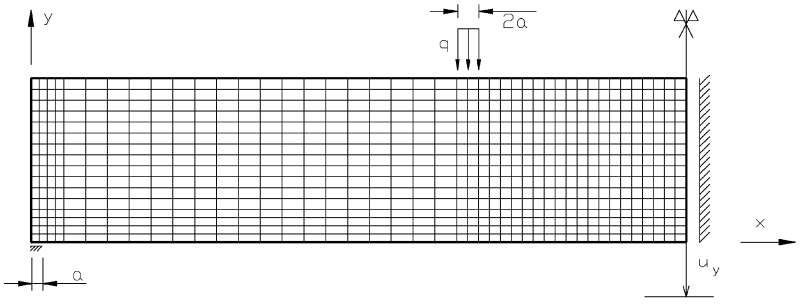

(a) Mesh I - 688 elements - $NDF = 1376$

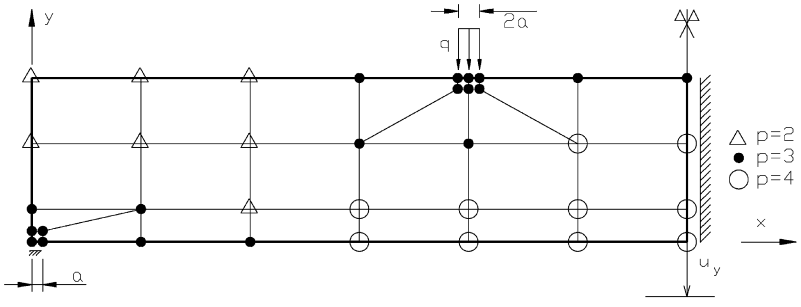

(b) Mesh II - 24 elements - $NDF = 392$

Fig. 3. Boundary conditions and adopted discretization (NDF = number of degrees of freedom, $a = 0.008\,333$ cm)

prescribed. Then, one step of 4% was applied, followed by 26 steps of 1% and 17 steps of 2% of the total loading. This peculiar form of applying the loading is due to the high nonlinearity observed after 12 kN;

stiffness matrix assemblage: in order to preserve stability of the numerical response, in the course of residual elimination, the stiffness was kept constant once a damage level ($D = 0.87$) was surpassed;

The nodal enrichment was not applied uniformly. Higher polynomial degrees were used at the nodes where the damage was highest. The final distribution for the polynomial degrees attached to the nodes is indicated in Fig. 3.

Figure 4 illustrates the confront between experimental measurements, [21], and numerical results. The curves describe the relationship between the applied load and displacement at a point in the middle section. Both simulations, conducted with conventional FEM and GFEM, are coincident and give results close to the experimental ones. The simulation was stopped at the loading level 30 kN due to the fact that plasticity of the steel was not considered.

Figures 5a and b present the damage distribution obtained in the simulations at a loading level of $F = 14.4$ kN. Close similarity in the damage distribution for the FEM and GFEM analysis can be observed. The FEM results are more localized, but complementary simulations with GFEM by imposing higher polynomial degrees also resulted in the same localized shape. On the basis of the promising results, an investigation about the possibility for an automatically nodal enrichment naturally appears. Accordingly, instead of fixing 'a priori' the polynomial degrees, a control over the approximation error could be used to drive the enrichment. This idea is developed in the following.

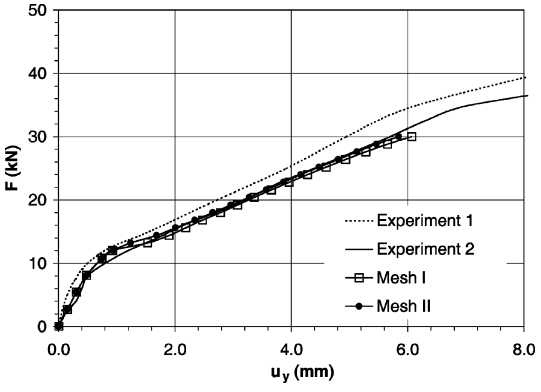

Fig. 4. Static analysis

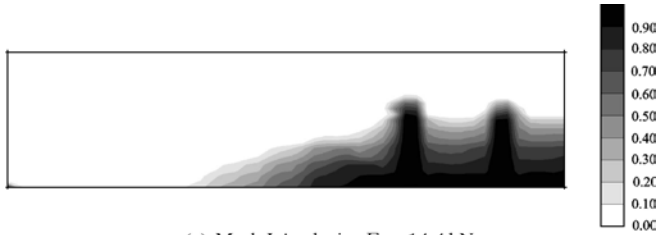

(a) Mesh I Analysis- $F = 14.4$ kN

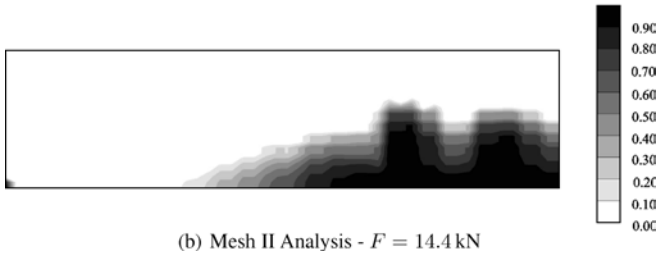

(b) Mesh II Analysis - $F = 14.4$ kN

Fig. 5. Damage distribution

6
Error measure

A p-adaptive procedure, tailored to the GFEM approach, needs a nodal error indicator. Here, this is obtained by considering such measure as an average value of the approximation error estimated on the boundaries and in the interior of the elements that share each vertex node. As a consequence, the contribution of the enrichment functions of each cloud is evaluated by the error indicator of the elements contained by the associated cloud. Aiming to determine the error measure of the elements it was adopted the element residual method (ERM), following the formulation presented in [7] and extended in [23, 24] to take into account the nonlinear aspects of the problem.

Accordingly, the space of approximating polynomial functions is preliminarily stated at the element level, being represented by $\mathscr{X}_p(\mathscr{K}) = \{\mathbf{v}_p \in \mathscr{H}^1; \mathbf{v}_p|_{\mathscr{K}} \in \mathscr{P}_p,\ \mathscr{K} \in \Omega\}$, where $\mathbf{v}_p|_{\mathscr{K}}$ refers to the restriction of the function $\mathbf{v}_p$ to the element $\mathscr{K} \in \Omega$ and $\mathscr{P}_p$ is the complete polynomial space of maximum degree p.

We denote the Galerkin's approximation of the problem (9) obtained at the load step $t + \Delta t$ by ${}^{t+\Delta t}\mathbf{u}_p$. The respective error of approximation is defined as:

$$ {}^{t+\Delta t}\mathbf{e}_p = {}^{t+\Delta t}\mathbf{u} - {}^{t+\Delta t}\mathbf{u}_p \quad \text{with} \quad {}^{t+\Delta t}\mathbf{e}_p \in \mathscr{H}^1 \tag{17} $$

One important aspect is that the nonlinear material behaviour of the medium implies that $\boldsymbol{\sigma}({}^{t+\Delta t}\mathbf{u}) - \boldsymbol{\sigma}({}^{t+\Delta t}\mathbf{u}_p) \neq \boldsymbol{\sigma}({}^{t+\Delta t}\mathbf{e}_p)$, thus increasing the difficulties of the error analysis. One way to overcome this problem consists in assuming a continuous stiffness variation with the numerical refinement. Then the following relation can be used:

$$ \boldsymbol{\sigma}({}^{t+\Delta t}\mathbf{u}) - \boldsymbol{\sigma}({}^{t+\Delta t}\mathbf{u}_p) \approx \left.\frac{\partial \boldsymbol{\sigma}}{\partial \boldsymbol{\varepsilon}}\right|_{{}^{t+\Delta t}\mathbf{u}_p} \boldsymbol{\varepsilon}\underbrace{({}^{t+\Delta t}\mathbf{u} - {}^{t+\Delta t}\mathbf{u}_p)}_{{}^{t+\Delta t}\mathbf{e}_p} \tag{18} $$

where $\partial\boldsymbol{\sigma}(\mathbf{u})/\partial\boldsymbol{\varepsilon}|_{{}^{t+\Delta t}\mathbf{u}_p}$ stands for the local stiffness associated to the solution ${}^{t+\Delta t}\mathbf{u}_p$.

Replacing then (17) and (18) into (9) a new BVP results, now leading to an estimate ${}^{t+\Delta t}\mathbf{e}_p^*$ to the discretization error ${}^{t+\Delta t}\mathbf{e}_p$:

$$ \begin{aligned} &\nabla^T \left[\left.\frac{\partial \boldsymbol{\sigma}}{\partial \boldsymbol{\varepsilon}}\right|_{{}^{t+\Delta t}\mathbf{u}_p} \boldsymbol{\varepsilon}({}^{t+\Delta t}\mathbf{e}_p^*)\right] + \mathbf{r}_\Omega({}^{t+\Delta t}\mathbf{u}_p) = \mathbf{0} \quad \text{in} \quad \Omega \\ &{}^{t+\Delta t}\mathbf{e}_p^* = \mathbf{0} \quad \text{in} \quad \Gamma_D \\ &\left[\left.\frac{\partial \boldsymbol{\sigma}}{\partial \boldsymbol{\varepsilon}}\right|_{{}^{t+\Delta t}\mathbf{u}_p} \boldsymbol{\varepsilon}({}^{t+\Delta t}\mathbf{e}_p^*)\right]\mathbf{n} = \mathbf{r}_\Gamma({}^{t+\Delta t}\mathbf{u}_p) \quad \text{in} \quad \Gamma_N \end{aligned} \tag{19} $$

where the volume and boundary residual functions are respectively given by:

$$ \begin{aligned} &\mathbf{r}_\Omega({}^{t+\Delta t}\mathbf{u}_p) \overset{\text{def}}{=} \nabla^T \boldsymbol{\sigma}({}^{t+\Delta t}\mathbf{u}_p) + {}^{t+\Delta t}\mathbf{b} \quad \text{in} \quad \Omega \\ &\mathbf{r}_\Gamma({}^{t+\Delta t}\mathbf{u}_p) \overset{\text{def}}{=} {}^{t+\Delta t}\hat{\mathbf{t}} - \mathbf{t}({}^{t+\Delta t}\mathbf{u}_p) \quad \text{in} \quad \Gamma_N \end{aligned} \tag{20} $$

Here, it is assumed that the essential boundary conditions are exactly satisfied.

Due to the linearization imposed by (18), the quality of the error estimation becomes strongly dependent on the closeness of the functions ${}^{t+\Delta t}\mathbf{u}$ and ${}^{t+\Delta t}\mathbf{u}_p$. Such a condition can be met by providing a sufficiently small load step.

The problem (19) can now be locally formulated in each element aiming to achieve local measures of the error. However, a new natural boundary condition must be imposed at the edges between the element $\mathscr{K}$ and the neighboring elements, $(\partial\mathscr{K} \setminus \partial\Omega)$. This condition is related to the jump in the traction vectors between adjacent elements. Moreover, as the true traction is unknown on $\partial\mathscr{K} \setminus \partial\Omega$, it is assumed that it can be estimated by the average of the approximate tractions $\langle \mathbf{t}({}^{t+\Delta t}\mathbf{u}_p)\rangle_m$ evaluated by taking the values defined at $\mathscr{K}$ and its neighboring elements. Therefore the new boundary condition can be given by:

$$ \left[\left.\frac{\partial \boldsymbol{\sigma}}{\partial \boldsymbol{\varepsilon}}\right|_{{}^{t+\Delta t}\mathbf{u}_p} \boldsymbol{\varepsilon}({}^{t+\Delta t}\mathbf{e}_p^*)\right]\mathbf{n} = \langle \mathbf{t}({}^{t+\Delta t}\mathbf{u}_p)\rangle_m - \mathbf{t}({}^{t+\Delta t}\mathbf{u}_p) \quad \text{on} \ \ \partial\mathscr{K} \setminus \partial\Omega \tag{21} $$

Now, the weak solution can be searched for. In [7], the Galerkin approximate form of a linear error estimator problem is accomplished by taking the bubble-like function space. Here, an analogous space can be built by using the set of shape functions of the GFEM. In this case, the local character of each function is acquired by considering its respective compact support, following the concept illustrated in Fig. 1. Taking the previous considerations into account, the bubble-like function space, named $\mathscr{X}^0_{p+1}$, can be defined by using the GFEM shape functions as:

$$ \mathscr{X}^0_{p+1}(\mathscr{K}) = \left\{\mathbf{v}^0_{p+1} \in \mathscr{X}_{p+1}(\mathscr{K}); \boldsymbol{\Pi}_p(\mathbf{v}^0_{p+1}) = 0;\ \mathbf{v}^0_{p+1} = 0 \quad \text{on} \ \ \partial\mathscr{K} \cap \Gamma_D\right\} \tag{22} $$

where $\boldsymbol{\Pi}_p : \mathscr{H}^r(\mathscr{K}) \to \mathscr{X}_p(\mathscr{K})$ is the local interpolation operator and r is defined according to [7]. Presently, instead of $\mathscr{H}^r(\mathscr{K})$, the polynomial space $\mathscr{X}_{p+1}(\mathscr{K}) \subset \mathscr{H}^r(\mathscr{K})$ is used, as it is assumed that the most important part of the error can be represented by the monomial terms one degree higher than those of the approximate solution space $\mathscr{X}_p(\mathscr{K})$ of $\mathbf{u}_p$. This assumption produces the space $\mathscr{X}^0_{p+1}(\mathscr{K})$ (the kernel of the operator $\boldsymbol{\Pi}_p$) spanned by the functions $\mathbf{v}^0_{p+1}$ that belong to the space $\mathscr{X}_{p+1}(\mathscr{K})$ and vanish on the boundary Γ_D. Summarizing, what is being considering is the projection of the error onto the space $\mathscr{X}^0_{p+1}(\mathscr{K})$. Such space can be generated, in the case of the GFEM, by the shape functions (2) as it will be described on what follows.

A new boundary value problem, for each element $\mathscr{K}$, can now be written in the variational form as:

Find ${}^{t+\Delta t}\tilde{\mathbf{e}}_p \in \mathscr{X}^0_{p+1}(\mathscr{K})$ such that:

$$ \mathscr{B}^{\text{tg}}_{\mathscr{K}}({}^{t+\tilde{\Delta t}}\tilde{\mathbf{e}}_p, \mathbf{v}^0_{p+1}) = \mathscr{L}_{\mathscr{K}}(\mathbf{v}^0_{p+1}) \quad \forall\ \mathbf{v}^0_{p+1} \in \mathscr{X}^0_{p+1}(\mathscr{K}) \tag{23} $$

where

$$\mathscr{B}^{\mathrm{tg}}_{\mathscr{K}} \overset{\mathrm{def}}{=} \iint_{\mathscr{K}} \boldsymbol{\varepsilon}^T(\mathbf{v}^0_{p+1})\boldsymbol{\sigma}^{\mathrm{tg}}({}^{t+\Delta t}\tilde{\mathbf{e}}_p) l_z \,\mathrm{d}x\,\mathrm{d}y \tag{24}$$

$$\begin{aligned}\mathscr{L}_{\mathscr{K}}(\mathbf{v}^0_{p+1}) \overset{\mathrm{def}}{=} & \iint_{\mathscr{K}} (\mathbf{v}^0_{p+1})^T({}^{t+\Delta t}\mathbf{b}) l_z \,\mathrm{d}x\,\mathrm{d}y \\ & - \mathscr{B}_{\mathscr{K}}({}^{t+\Delta t}\mathbf{u}_p, \mathbf{v}^0_{p+1}) \\ & + \int_{\partial\mathscr{K}\cap\Gamma_N} (\mathbf{v}^0_{p+1})^T({}^{t+\Delta t}\hat{\mathbf{t}}) l_z \,\mathrm{d}s \\ & + \int_{\partial\mathscr{K}\setminus\partial\Omega} (\mathbf{v}^0_{p+1})^T \left\langle \mathbf{t}({}^{t+\Delta t}\mathbf{u}_p)\right\rangle_m l_z \,\mathrm{d}s \end{aligned} \tag{25}$$

and

$$\boldsymbol{\sigma}^{\mathrm{tg}}({}^{t+\Delta t}\tilde{\mathbf{e}}_p) = \left.\frac{\partial\boldsymbol{\sigma}(\mathbf{u}_p)}{\partial\boldsymbol{\varepsilon}}\right|_{{}^{t+\Delta t}\mathbf{u}_p} \boldsymbol{\varepsilon}({}^{t+\Delta t}\tilde{\mathbf{e}}_p) \tag{26}$$

In the above formulation, ${}^{t+\Delta t}\tilde{\mathbf{e}}_p$ is the Galerkin approximation of the error function ${}^{t+\Delta t}\mathbf{e}^*_p$, actually defining the error indicator function and $\mathbf{v}^0_{p+1}$ is the test function of the problem. Both of them are described by the GFEM functions as:

$${}^{t+\Delta t}\tilde{\mathbf{e}}_p = (\boldsymbol{\Phi}^0_{p+1})^T {}^{t+\Delta t}\mathbf{I} \quad \mathbf{v}^0_{p+1} = (\boldsymbol{\Phi}^0_{p+1})^T\mathbf{V}^0 \tag{27}$$

where the vector $\boldsymbol{\Phi}^0_{p+1}$ is built by the set of shape functions of the expression (2), after eliminating from the set $\{\phi^{p+1}_{ji}\}$ the terms of the subset $\{\phi^p_{ji}\}$. Here the functions L_{ij} are defined by the set of monomials required to reproduce exactly complete polynomials of $p+1$ degree, in the case of the set $\{\phi^{p+1}_{ji}\}$, and p in the case of the set $\{\phi^p_{ji}\}$. ${}^{t+\Delta t}\mathbf{I}$ and $\mathbf{V}^0$ are nodal parameter vectors associated to each shape function of the set $\mathscr{X}^0_{p+1}(\mathscr{K})$. The vector ${}^{t+\Delta t}\mathbf{I}$ is the vector of error indicators.

The above problem results in the following system of equations, to each element $\mathscr{K}$:

$${}^{t+\Delta t}\mathbf{K}^{\mathscr{K}}_{\mathrm{er}}\,{}^{t+\Delta t}\mathbf{I}^{\mathscr{K}} = {}^{t+\Delta t}\mathbf{R}^{\mathscr{K}} \tag{28}$$

where $\mathbf{I}^{\mathscr{K}}$ is the vector of error indicators and one employs:

- the stiffness matrix (in which $\mathbf{C}_{\mathrm{tg}}$ stands for the tangent modulus expression of the Mazars' constitutive damage model, [23]) given by:

$${}^{t+\Delta t}\mathbf{K}^{\mathscr{K}}_{\mathrm{er}} = \iint_{\mathscr{K}} (\mathbf{B}^0_{p+1})^T {}^{t+\Delta t}\mathbf{C}_{\mathrm{tg}}\mathbf{B}^0_{p+1} l_z \,\mathrm{d}x\,\mathrm{d}y \ ; \tag{29}$$

  with

$$\mathbf{B}^0_{p+1} = \mathbf{L}(\boldsymbol{\Phi}^0_{p+1})^T \tag{30}$$

- the generalized vector of the residual forces:

$$\begin{aligned}{}^{t+\Delta t}\mathbf{R}^{\mathscr{K}} = & \iint_{\mathscr{K}} (\boldsymbol{\Phi}^0_{p+1})^T {}^{t+\Delta t}\mathbf{b} l_z \,\mathrm{d}x\,\mathrm{d}y \\ & + \int_{\partial\mathscr{K}} (\boldsymbol{\Phi}^0_{p+1})^T {}^{t+\Delta t}\boldsymbol{\theta}^{\mathscr{K}} l_z \,\mathrm{d}s \\ & + \int_{\partial\mathscr{K}\cap\Gamma_N} (\boldsymbol{\Phi}^0_{p+1})^T {}^{t+\Delta t}\hat{\mathbf{t}} l_z \,\mathrm{d}s \\ & + \int_{\partial\mathscr{K}\setminus\partial\Omega} (\boldsymbol{\Phi}^0_{p+1})^T \left\langle \mathbf{t}({}^{t+\Delta t}\mathbf{u}_p)\right\rangle_m l_z \,\mathrm{d}s \\ & - \iint_{\mathscr{K}} \boldsymbol{\varepsilon}^T(\boldsymbol{\Phi}^0_{p+1})\boldsymbol{\sigma}(\boldsymbol{\Phi}^0_{p+1}) l_z \,\mathrm{d}x\,\mathrm{d}y\, {}^{t+\Delta t}\mathbf{U} \end{aligned} \tag{31}$$

At this point, a comment regarding the introduction of the vector ${}^{t+\Delta t}\theta^{\mathscr{K}}$ appearing in (31) should be given. The BVP (19), corresponds to a Neumman problem as it is formulated at the element level and involving only natural boundary conditions. Except for the elements intersecting the boundary $\partial\Omega$ this formulation is somewhat unsatisfactory due to the possible lack of continuity. As a consequence the problem to be approximated may not have an unique solution. In order to guarantee the uniqueness of the solution, one strong requirement is that the boundary data $\mathbf{r}_\Gamma$, $\mathbf{t}({}^{t+\Delta t}\mathbf{u}_p)$ and $\left\langle \mathbf{t}({}^{t+\Delta t}\mathbf{u}_p)\right\rangle_m$ be in equilibrium with the interior residual $\mathbf{r}_\Omega$. This is accomplished, for instance by following the strategy proposed in [9]. Such strategy consists of introducing a new traction distribution $\theta(\mathbf{x})$ along the boundary of each element $\mathscr{K}$ in order to equilibrate the original set of boundary data. This traction distribution is defined such that, at each element $\mathscr{K}$, the corresponding set of vectors ${}^{t+\Delta t}\mathbf{R}^{\mathscr{K}}_j$, associated to the nodes $j \in \mathscr{K}$, produces null force and moment resultants. To achieve this condition only the components of ${}^{t+\Delta t}\mathbf{R}^{\mathscr{K}}_j$ related to the PU functions are necessary. In fact, the other components, associated to the enrichment functions, are self-equilibrated and take no part in this procedure. The new boundary data obtained leads, at the end of the step $t+\Delta t$, to the vector ${}^{t+\Delta t}\theta^{\mathscr{K}}$. More details about this issue, specially related to the GFEM approach can be found in [23, 24].

Once the function ${}^{t+\Delta t}\tilde{\mathbf{e}}_p$ is obtained for each element, local values of the energy norm $\tilde{\mathscr{E}}_{\mathscr{K}} \overset{\mathrm{def}}{=} \|{}^{t+\Delta t}\tilde{\mathbf{e}}_p\|_{\mathscr{U}(\mathscr{K})} = \left[\iint_{\mathscr{K}} \boldsymbol{\varepsilon}^T({}^{t+\Delta t}\tilde{\mathbf{e}}_p)\boldsymbol{\sigma}({}^{t+\Delta t}\tilde{\mathbf{e}}_p) l_z \,\mathrm{d}x\,\mathrm{d}y\right]^{1/2}$ can be estimated and the error indicators by element can be defined. The local measure consistent with GFEM can then be formulated by defining the error indicator at each cloud as:

$$\tilde{\mathscr{E}}_{\omega_j} \overset{\mathrm{def}}{=} \sum_{\mathscr{K}\in\omega_j} V_{\mathscr{K}} \|{}^{t+\Delta t}\tilde{\mathbf{e}}_p\|_{\mathscr{U}(\mathscr{K})} / V_{\omega_j} \tag{32}$$

where $V_{\omega_j} = \sum_{\mathscr{K}\in\omega_j} V_{\mathscr{K}}$ and $V_{\mathscr{K}}$ are the volumes of the cloud and the element respectively. In fact, the expression (32) corresponds to the average of the values found at each element that shares the vertex node of the cloud, weighted by the respective volume.

Finally, the global measure that represents the estimated error can be defined as the sum of the local values evaluated at each element $\mathscr{K}$:

$$\|{}^{t+\Delta t}\tilde{\mathbf{e}}_p\|_{\mathscr{U}} \overset{\mathrm{def}}{=} \sqrt{\sum_{\mathscr{K}\in\Omega} \tilde{\mathscr{E}}^2_{\mathscr{K}}} \tag{33}$$

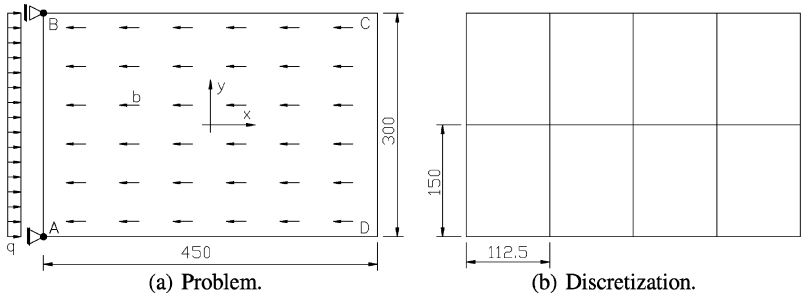

(a) Problem. (b) Discretization.

Fig. 6. Concrete plate – $E = 29\,200$ MPa, $\nu = 0.2$

6.1
Effectivity index of the global error measure: a numerical example

In order to look at the quality of the adopted error measure as an estimation of the global error, ${}^{t+\Delta t}\mathbf{e}_p$, an example illustrated in Fig. 6a is solved. The example consists of a concrete plate under plane stress conditions and subjected to compression body forces ($b = 1000$ kN/m^3). The natural boundary condition is represented by the distributed force ($q = 450$ kN/m^2) along side AB. The material behaviour is simulated by the Mazars' Damage model with local approach ($r_{\mathrm{nl}} = 0$), being the values for the parameters adopted as: $A_T = 0.7$, $B_T = 8000$, $A_C = 0.85$, $B_C = 1050$ and $\varepsilon_{\mathrm{d0}} = 0.000067$. The exact reference solution is assumed to be the numerical solution obtained by a discretization of 2400 bi-linear elements. Such conclusion was stated after several numerical tests that show a convergence of the results for the one found with this discretization. The global error is then estimated using the mesh depicted in Fig. 6b and composed of bi-linear elements without considering polynomial enrichment, as the aim is only to verify the effectivity of the global measure.

At the end of each load step, the error is estimated by the measure (33) and compared to the following inner product:

$$
{}^{t+\Delta t}(\boldsymbol{\sigma}_{\mathrm{er}}, \boldsymbol{\varepsilon}_{\mathrm{er}}) = \sqrt{\iint_{\Omega} [\boldsymbol{\sigma}({}^{t+\Delta t}\mathbf{u}) - \boldsymbol{\sigma}({}^{t+\Delta t}\mathbf{u}_p)][\boldsymbol{\varepsilon}({}^{t+\Delta t}\mathbf{u} - {}^{t+\Delta t}\mathbf{u}_p)] l_z \, \mathrm{d}x \, \mathrm{d}y} \tag{34}
$$

where $\mathbf{u}$ stands for the adopted exact solution. In estimating the error at each element $\mathscr{K}$, the space $\mathscr{X}_2^0(\mathscr{K}) = \{\mathbf{v}_2^0 \in \mathscr{X}_2(\mathscr{K}) \subset \mathscr{H}^1;\ \Pi_p(\mathbf{v}_2^0) = 0,\ \mathbf{v}_2^0 = 0 \text{ in } \Gamma_D\}$ is employed.

The global effectivity index θ is given by the ratio between the two measures (33) and (34). Such an index results always close to the unity for each load step, as it is shown in Fig. 7. As a conclusion, the norm (33) estimates the error measure very well, at least for this kind of problem.

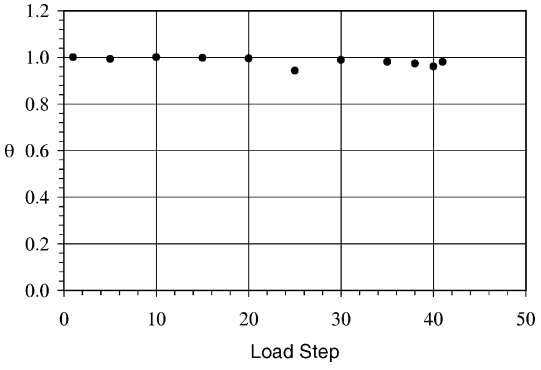

Fig. 7. Global effectivity index at the end of each load step

7
A proposition for *p*-adaptivity

A small value for the error measure defined in the Sec. 6 must not be confused with a guarantee for a precise description of the structural behaviour along the loading history, since the errors due to integration processes are not considered here. The aim of the adaptive refinement proposed here, and summarized in the algorithm 1, is to control only the error of the approximation at the end of each load step, i.e. $\|{}^{t+\Delta t}\tilde{\mathbf{e}}_p\|_{\mathscr{U}}$, by keeping it at a sufficiently small value.

As a part of the strategy proposed here, after equilibrium be verified at the load step $t + \Delta t$, the measure $\|{}^{t+\Delta t}\tilde{\mathbf{e}}_p\|_{\mathscr{U}}$ is computed for each cloud. The option to clouds is justified by its consistence with GFEM treatment. This option is summarized in the algorithm 2. Accordingly, a new loading step can be applied only if the maximum error comparing all the clouds is lower than a certain tolerance $\mathrm{TOL}_{\mathrm{er}}$. A refinement of the PU functions should be conducted based on the cloud error indicators. Once a new enriched approximation is defined, the present load step must be repeated. But, in order to do that, the results obtained for the previous load step must be made compatible with the set of additional degrees of freedom introduced by the new approximation and with the necessary quadrature order of integration, as well. The sequence of refinement, data transference and re-equilibrium analysis is repeated until the tolerance is met. The strategy adopted for such transference is described in the next section.

7.1
On the transference of variables

By conducting a nonlinear analysis by GFEM and supposing that at the end of some load step a refinement action is indicated by the adaptive procedure, the number of nodal degrees of freedom and also the

Algorithm 1. *p*-adaptive algorithm – nonlinear analysis

Read the data for the geometry, loading and approximation
Read υ, TOL_{er}, $TOL_{\mathscr{U}}$, p_{max}, i_p
$t = 1$, $\Delta t = 1$
{*Load step application*}
repeat
{*Adaptive procedure*}
loop
Assemble ${}^{t+\Delta t}\Delta F, {}^{t+\Delta t}F_{\text{ext}}, {}^{t+\Delta t}K_{\text{sec}}^{(0)}$
Solve the system ${}^{t+\Delta t}K_{\text{sec}}^{(0)}\Delta U^{(0)} = {}^{t+\Delta t}\Delta F$
Update ${}^{t+\Delta t}U^{(0)}$
Calculate the damage
Assemble ${}^{t+\Delta t}F_{\text{int}}^{(0)}$
Calculate $\psi^{(0)} = {}^{t+\Delta t}F_{\text{ext}} - {}^{t+\Delta t}F_{\text{int}}^{(0)}$
$i_t = 0$
{*Newton-Raphson Iterative Procedure*}
repeat
$i_t = i_t + 1$
Assemble ${}^{t+\Delta t}K_{\text{sec}}^{(i_t)}$
Solve the system ${}^{t+\Delta t}K_{\text{sec}}^{(i_t)}\ \Delta U^{(i_t)} = \psi^{(i_t)}$
Update ${}^{t+\Delta t}U^{(i_t)}$
Calculate the damage
Assemble ${}^{t+\Delta t}\ F_{\text{int}}^{(i_t)}$
Calculate $\psi^{(i_t)} = {}^{t+\Delta t}F_{\text{ext}} - {}^{t+\Delta t}F_{\text{int}}^{(i_t)}$
until $(\Delta U^{(i_t)})^T\boldsymbol{\psi}^{(i_t-1)} < TOL_{\mathscr{U}}$
Algorithm 2 {*Error evaluation and refinement if necessary*}
Directly transfer the nodal parameters to the new vector ${}^{t}\mathbf{U}^{(i_t)}$
Transfer the damage and associated parameters to the new integration points
Algorithm 3 {*Proceed with a new equilibration of the load step t*}
endloop
$t = t + \Delta t$
until the last load step be reached

number of integration points increases. In particular, the change on the number of integration points aims to guarantee precision of the integration based on the Gaussian Quadrature. Prior proceeding with the analysis by reapplying the same load step, a consistent procedure for transference of information from the old to the new set of variables becomes necessary. In GFEM the transference of information attached to the nodal parameters does not require any special strategy, as the improved approximation contains the old set of degrees of freedom. To illustrate this let's consider a cloud ω_j where the sets of approximation functions and nodal parameters are represented as follows:

$$(\boldsymbol{\Phi}_p)_j^T = \begin{bmatrix} \mathscr{N}_j & 0 & p_{j2}\mathscr{N}_j & 0 & \cdots & 0 & p_{jq_j(p)}\mathscr{N}_j & 0 \\ 0 & \mathscr{N}_j & 0 & p_{j2}\mathscr{N}_j & 0 & \cdots & 0 & p_{jq_j(p)}\mathscr{N}_j \end{bmatrix} \tag{35}$$

$$\mathbf{U}^T = \begin{bmatrix} u_j^x & u_j^y & b_{j2}^x & b_{j2}^y & \cdots & b_{jq_j}^x & b_{jq_j}^y \end{bmatrix} \tag{36}$$

After refinement leading to an approximation of order $p+1$ the matrix of basis functions assumes the form:

$$ {}^{\text{new}}(\boldsymbol{\Phi}_p)_j^T = \underbrace{\begin{bmatrix} \mathscr{N}_j & 0 & p_{j2}\mathscr{N}_j & 0 & \cdots & 0 & p_{jq_j(p)}\mathscr{N}_j & 0 \\ 0 & \mathscr{N}_j & 0 & p_{j2}\mathscr{N}_j & 0 & \cdots & 0 & p_{jq_j(p)}\mathscr{N}_j \end{bmatrix}}_{(\boldsymbol{\Phi}_p)_j^T} $$

$$ \underbrace{\begin{bmatrix} p_{jq_j(p)+1}\mathscr{N}_j & 0 & \cdots & 0 & p_{jq_j(p+1)}\mathscr{N}_j & 0 \\ 0 & p_{jq_j(p)+1}\mathscr{N}_j & 0 & \cdots & 0 & p_{jq_j(p+1)}\mathscr{N}_j \end{bmatrix}}_{\text{additional functions}} $$

The new set of functions contains the old one as can be noted. As a consequence the expanded vector of nodal parameters is built by direct transference of the old one and by attribution of null values to the added parameters.

Algorithm 2. Algorithm that evaluates the error and invoques the p-refinement – load step $t + \Delta t$

for $\mathscr{K} = 1$ to NEL **do**
  Assemble ${}^{t+\Delta t}\mathbf{K}_{\text{er}}^{\mathscr{K}}, {}^{t+\Delta t}\boldsymbol{\theta}^{\mathscr{K}}\, e^{t+\Delta t}\mathbf{R}_{\text{equi}}^{\mathscr{K}}$
  Solve the system ${}^{t+\Delta t}\mathbf{K}_{\text{er}}^{\mathscr{K}}\, {}^{t+\Delta t}\mathbf{I}^{\mathscr{K}} = {}^{t+\Delta t}\mathbf{R}_{\text{equi}}^{\mathscr{K}}$
  Calculate ${}^{t+\Delta t}\tilde{\mathscr{E}}_{\mathscr{K}} = \|{}^{t+\Delta t}\tilde{\mathbf{e}}_p\|_{\mathscr{U}(\mathscr{K})}$
  $\|{}^{t+\Delta t}\tilde{\mathbf{e}}_p\|_{\mathscr{U}}^2 = \|{}^{t+\Delta t}\tilde{\mathbf{e}}_p\|_{\mathscr{U}}^2 + \left({}^{t+\Delta t}\tilde{\mathscr{E}}_{\mathscr{K}}\right)^2$
end for
$\|{}^{t+\Delta t}\tilde{\mathbf{e}}_p\|_{\mathscr{U}} = \sqrt{\|{}^{t+\Delta t}\tilde{\mathbf{e}}_p\|_{\mathscr{U}}}$
$\tilde{\mathscr{E}}_{\%} = \|{}^{t+\Delta t}\tilde{\mathbf{e}}_p\|_{\mathscr{U}} / \|{}^{t+\Delta t}\mathbf{u}_p\|_{\mathscr{U}}$
if $\tilde{\mathscr{E}}_{\%} \leq TOL_{\text{er}}$ **then**
  Stop the analysis {*Adaptive procedure convergence*}
else
  $n_\upsilon = 0$
  $i_{end} = 0$
  repeat
    for $\omega_j = 1$ to N **do**
      Calculate $\tilde{\mathscr{E}}_{\omega_j} = \sum_{\mathscr{K}} \in \omega_j V_{\mathscr{K}} \tilde{\mathscr{E}}_{\mathscr{K}} / V_{\omega_j}$
    end for
    $\tilde{\mathscr{E}}_{max} = \max\left(\tilde{\mathscr{E}}_{\omega_j}, \omega_j = 1, \ldots, N\right)$
    for $\omega_j = 1$ to N **do**
      if $\tilde{\mathscr{E}}_{\omega_j} \geq \upsilon \tilde{\mathscr{E}}_{max}$ **then**
        if $p_{\omega_j} < p_{max}$ **then**
          $p_{\omega_j} = p_{\omega_j} + i_p$ {*Enrichment of the cloud* ω_j}
          $n_\upsilon = 1$
        else
          $i_{end} = i_{end} + 1$
        end if
      end if
    end for
    if $i_{end} = N$ **then**
      Stop the analysis {The TOL_{er} cannot be reached}
    else if $n_\upsilon = 0$ **then**
      update υ to 90% of its value
    end if
  until $n_\upsilon = 1$
end if

Algorithm 3. New equilibration of the load step t

Calculate the damage
Assemble ${}^t\boldsymbol{F}_{\text{int}}^{(0)}$, ${}^t\boldsymbol{F}_{\text{ext}}^{(0)}$
Calculate $\psi^{(0)} = {}^t\boldsymbol{F}_{\text{ext}} - {}^t\boldsymbol{F}_{\text{int}}^{(0)}$
$i_t = 0$
{*Newton-Raphson iterative procedure*}
repeat
  $i_t = i_t + 1$
  Assemble ${}^t\boldsymbol{K}_{\text{sec}}^{(i_t)}$
  Solve the system ${}^t\boldsymbol{K}_{\text{sec}}^{(i_t)} \Delta \boldsymbol{U}^{(i_t)} = \psi^{(i_t)}$
  Update ${}^t\boldsymbol{U}^{(i_t)}$
  Calculate the damage
  Assemble ${}^t\boldsymbol{F}_{\text{int}}^{(i_t)}$
  Calculate $\psi^{(i_t)} = {}^t\boldsymbol{F}_{\text{ext}} - {}^t\boldsymbol{F}_{\text{int}}^{(i_t)}$
until $\Delta \mathbf{U}^{(i_t)^T} \psi^{(i_t - 1)} < TOL_{\mathscr{U}}$

Related to the set of sample points for integration by Gauss Quadrature the strategy to be adopted for variable transference requires a certain criterion. In fact, some of the variables attached to that points, as the damage values, have direct influence over the nonlinear structural behaviour. The strategy suggested here is detailed in [23, 25] and can be summarized as follows. The old set of integration points can be used to build a function describing the damage distribution over each cloud. It is a simple procedure of fitting a function to a set of variables associated to a set of positions and can be performed, for example, by adopting the least square method for each cloud separately. As a consequence of such local procedure, the the variable damage at a single element has several descriptions, each one associated to one of the nodes of such element. An unique and global description can be achieved by multiplying the functions of each cloud by the corresponding PU function and summing the resulting product. Essentially, the PU concept is used just like in the definition of the GFEM approximation to impose the continuity over local descriptions of the variable damage. From this description the values of the variables attached to the new Gauss points can be obtained. However, the equilibrium verified with the old set of variables can be violated by assuming the new one. Thus, after the variables transference, the equilibrium analysis to the step t must be restarted as indicated by algorithm 3. In this way the displacement field results become compatible with the new nodal parameters and quadrature order.

7.2 Numerical Example

The problem illustrated by the Fig. 8a was originally proposed in [19] and corresponds to a notched concrete plate of thickness $l_z = 12$ cm, subjected to two equal and opposite horizontal forces F. The presence of the notch induces the formation and growth of a damage zone around and ahead its extremity.

The numerical analysis was performed under plane strain conditions, considering monotonical loading and limited to the onset and growth of damage stages up to the maximum load capacity of the structure. The nonlocal approach was employed with the radius $r_{\text{nl}} = 1.5$ cm. The parameters of the Mazars' damage model related to the kind of concrete considered are: $A_T = 0.8$, $B_T = 20\,000$, $A_C = 1.4$, $B_C = 1850$ and $\varepsilon_{d0} = 0.000\,123$.

The discretization and boundary conditions adopted are depicted in the Fig. 9. The distribution of the polynomial enrichment was determined by the adaptive algorithm proposed in [7] and fitted to the nonlinear case in [23]. The error indicator associated with each cloud was employed. The maximum value computed among all clouds was compared to the other ones indicating which cloud should have its local approximation improved. A polynomial enrichment was then performed, i.e., the polynomial degree of the present approximation was

$$ {}^{\text{new}}\mathbf{U}^T = \underbrace{\left[u_j^x\, u_j^y\, b_{j2}^x\, b_{j2}^y \cdots b_{jq(p)_j}^x\, b_{jq(p)_j}^y\right.}_{\mathbf{U}^T} \underbrace{\left. b_{jq(p)_j+1}^x = 0\, b_{jq(p)_j+1}^y = 0 \cdots b_{jq(p_j+1)}^x = 0\, b_{jq(p_j+1)}^y = 0\right]}_{\text{added parameters}} \tag{37} $$

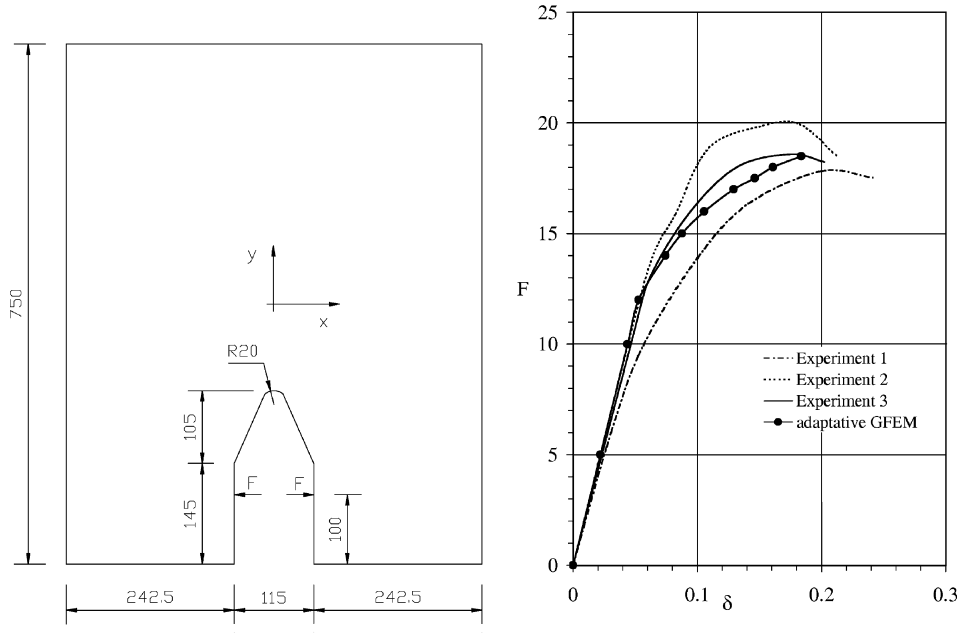

(a) Geometry and applied loading. (b) Global response.

Fig. 8. Notched concrete plate – $E = 30\,000$ MPa and $\nu = 0.2$– measures in mm

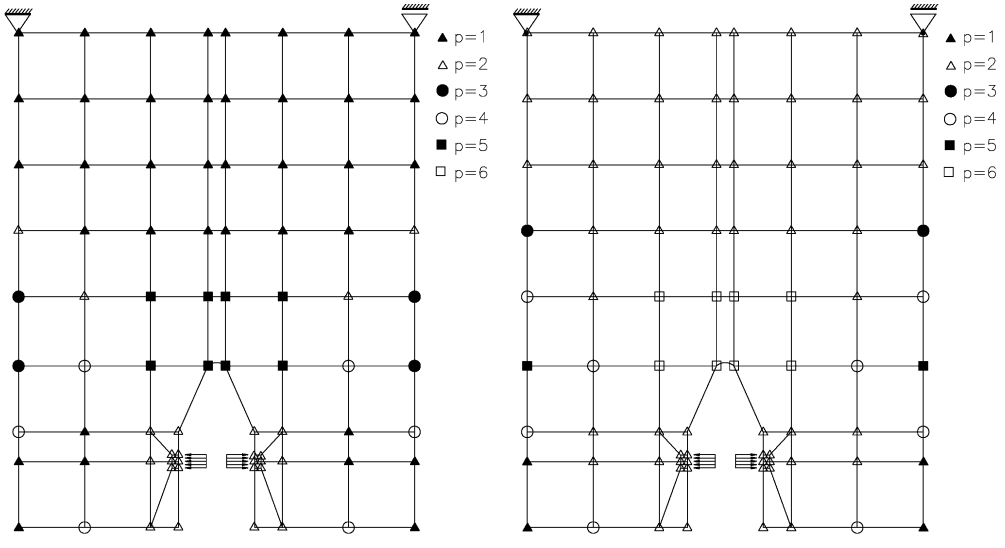

(a) Discretization used until step 7. (b) Discretization used after step 7.

Fig. 9. Discretization defined by the adaptive algorithm

increased by one degree. Such adaptive process was introduced into the incremental solution procedure of the nonlinear problem, being verified at the end of each load step. Additional details about the above concisely described strategy as well as the consistent procedure of variables transference can be found in [23, 25].

The tolerance of the Newton-Raphson iterative process was assumed to be 1% of the energy norm of the first elastic step. The force $F = 18.5$ kN was applied in 10 load steps (2 of 5 kN, 2 of 2 kN, 3 of 1 kN and 3 of 0.5 kN).

In the expression (29), the tangent constitutive relation was replaced by the secant one. This procedure was necessary in order to keep the matrix ${}^{t+\Delta t}\mathbf{K}_{er}^{\mathscr{K}}$ positive-definite, thus assuring the applicability of the error measure described in the Sect. 6 even in presence of damage. As a consequence, this error measure cannot be rigorously considered as a true error estimator. Nevertheless it can be employed in the adaptive procedure as error indicator guiding the nodal enrichment, as one can be observe by the results that follow. In the adaptive algorithm of [23], the parameters $\text{TOL}_{\text{error}} = 15\%$, $\upsilon = 0.5$ and $p_{\max} = 8$ were selected.

The numerical integration was performed by employing 4×4 Gauss-Lobatto points at the great majority of the elements, except those close to the notch where the 15×15 rule was used. Such procedure was adopted due to the high polynomial degree expected for the nodes belonging to that region and also to better simulate the damage evolution in it.

In Fig. 8b, the experimental [19] and numerical curves representing the global response in terms of the force F

and notch aperture δ are plotted. The adaptive process was characterized by two refinement stages. The first stage was trigged at the first elastic step leading to the discretization shown in Fig. 9a after a sequence of five iterations of the adaptive enrichment. Such discretization was again modified at the load step 7, when two more iterations were done to accomplished the final nodal enrichment depicted in the Fig. 9b.

Finally, an important issue was not considered here – the possibility of unrefining or even of unenriching the approximation in the clouds where the error indicator becomes much smaller than the average error looked for (in the sense of equally distributing of the error providing the optimal approximation). This fact was not observed in the present problem, but should be considered in a general implementation if the aiming is to propose an efficient adaptive procedure. Indeed, the *p*-unenrichment of the clouds is very straightforward as long as no restriction over the approximation has been imposed while performing the *p*-refining. On the other hand, the *h*-unrefining demands the introduction of a special strategy to treat this kind of problem. Even so, the using of the PU concept allows performing this task without penalizing the efficiency of the GFEM, [18, 26].

8
Final considerations

The fundamental feature of nodal enrichment presented by the GFEM, aiming to avoid mesh refinement, is very attractive for nonlinear analysis. Here this feature was explored by using this method in material nonlinear problems induced by progressive damage. In spite of the good response obtained by exploring the possibilities of using a coarse mesh and prefixing the nodal enrichment, the method naturally induces an adaptive strategy for p-refinement. The element residual method has been adapted in order to generate an error indicator. The residual element method fits very well with the nodal enrichment strategy of the GFEM, not only due to the very direct way of building the approximation space $\mathscr{X}_{p+1}$ but also by considering the manner in which the *p*-refinement is performed. The error indicator resulting from the adopted global error measure resulted in a good effectivity index, according to [23, 24], then motivating their employment as a guide in the *p*-adaptive procedure. The process suggested, based on the equidistribution of error indicators associated to the nodes, was illustrated by a final example.

Despite the good results obtained, the adaptive procedure deserves a valuation of the processing time, or even better, a floating point operations analysis, which was not conduct here. In fact, due to the sequence of refinement, data transference and re-equilibrium analysis required to complete the proposed procedure, the time of processing can become very long without an equivalent compensation on the accuracy improvement.

References

1. **Strouboulis T, Babuška, I, Copps K** (2000) The design and analysis of the generalized finite element method. Comput. Meth. Appl. Mech. Eng. 181(1–3): 43–69
2. **Duarte CA, Babuška I, Oden JT** (2000) Generalized finite element methods for three-dimensional structural mechanics problems. Comput. Struct. 77(2): 215–232
3. **Duarte CA, Oden, JT** (1996) An h-p adaptive method using cloud. Comput. Meth. Appl. Mech. Eng. 139: 237–262
4. **Oden JT, Reddy JN** (1976) An Introduction to the Mathematical Theory of Finite Elements, Pure and Applied Mathematics, John Willey &Sons Inc.
5. **Oden JT, Duarte CA** (1997) Clouds Cracks and fem's. In: Reddy BD (ed.), Recent Developments in Computational and Applied Mechanics, International Center for Numerical Methods in Engineering, CIMNE, Barcelona, Spain, pp. 302–321
6. **Duarte CA, Hamzeh ON, Liszka TJ, Tworzydlo WW** (2001) A generalized finite element method for the simulation of three-dimensional dynamic crack propagation, Comput. Meth. Appl. Mech. Eng. 190: 2227–2262
7. **Oden JT, Demkowicz L, Rachowicz W, Westermann TA** (1989) Toward a universal h-p adaptive finite element strategy, Part 2. A posteriori error estimation. Comput. Meth. Appl. Mech. Eng. 77: 113–180
8. **Ainsworth M, Oden JT** (1997) A posteriori error estimation in finite element analysis. Comput. Meth. Appl. Mech. Eng. 142: 1–88
9. **Ladevèze P, Maunder EAW** (1996) A general method for recovering equilibrating element tractions. Comput. Meth. Appl. Mech. Eng. 137: 111–151
10. **Babuška I, Caloz G, Osborn JE** (1994) Special finite element method for a classe of second order elliptic problems whith rough coefficients. SIAM J. Numer. Anal. 31(4): 745–981
11. **Melenk JM** (1995) On Generalized Finite Element Methods. PhD thesis, University of Maryland College Park
12. **Melenk JM, Babuška I** (1996) The partition of unity finite element method: Basic theory and applications. Comput. Meth. Appl. Mech. Eng. 39: 289–314
13. **Duarte CA, Oden JT** (1995) Hp clouds–a meshless method to solve boundary-value problem, Tech. rep., TICAM, The University of Texas at Austin, technical Report
14. **Duarte CA, Oden JT** (1996) H-p Clouds-an h-p meshless method. In: Numerical Methods for Partial Differential Equations, John Wiley &Sons Inc., pp. 1–34
15. **Oden JT, Duarte CA, Zienkiewicz OC** (1998) A new cloud-based hp finite element method. Comput. Meth. Appl. Mech. Eng. 153: 117–126
16. **Belytschko T, Black T** (1999) Elastic crack growth in finite elements with minimal remeshing. Int. J. Numer. Meth. Eng. 45: 601–620
17. **Moës N, Dolbow J, Belytschko T** (1999) A finite element method for crack growth without remeshing. Int. J. Numer. Meth. Eng. 46: 131–150
18. **Strouboulis T, Copps K, Babuška I** (2001) The generalized finite element method. Comput. Meth. Appl. Mech. Eng. 190: 4081–4193
19. **Mazars J** (1984) Application de la mécanique de l'endommagement au comportement non lineaire et à la rupture du béton de structure, Doutorado Université Paris 6
20. **Davenne L, Saouridis C, Piau JM** (1989) Un code de calcul pour la prévision du comportement de structures endommageables en béton en béton armé ou en béton de fibres, Tech. Rep. 478, Institut Technique du Batiment et des Travaux Publics, série: Béton 267
21. **Álvares MS** (1993) Study of a damage model to concrete: formulation parametric identification and simulation by the finite element method (in Portuguese), MSc. Dissertation, São Carlos Scholl of Engineering, University of São Paulo
22. **Ranjbaran A** (1991) Embedding of Reinforcements in Reinforced Concrete Elements Implemented in DENA. Comput. Struct. 40(4): 925–930

23. **Barros FB** (2002) Meshless Methods and Generalized Finite Element Method in Structural Nonlinear Analysis (in Portuguese), PhD thesis, São Carlos Scholl of Engineering, University of São Paulo
24. **Barros FB, Proença SPB, de Barcellos CS** (2002) On error estimator and *p*-adaptivity in the Generalized Finite Element Method. Int. J. Numer. Meth. Eng. (submitted)
25. **Barros FB, Proença SPB, de Barcellos CS** (2003) The generalized finite element method–discussions about a p-adaptivy strategy on structural nonlinear analysis (to be published)
26. **Duarte CA** (2002) Personal communication